
DeepMoM: Robust Deep Learning With Median-of-Means

Shih-Ting Huang

Department of Mathematics
Ruhr University, Bochum
shih-ting.huang@rub.de

Johannes Lederer

Department of Mathematics
Ruhr University, Bochum
johannes.lederer@rub.de

Abstract

Data used in deep learning is notoriously problematic. For example, data are usually combined from diverse sources, rarely cleaned and vetted thoroughly, and sometimes corrupted on purpose. Intentional corruption that targets the weak spots of algorithms has been studied extensively under the label of “adversarial attacks.” In contrast, the arguably much more common case of corruption that reflects the limited quality of data has been studied much less. Such “random” corruptions are due to measurement errors, unreliable sources, convenience sampling, and so forth. These kinds of corruption are common in deep learning, because data are rarely collected according to strict protocols—in strong contrast to the formalized data collection in some parts of classical statistics. This paper concerns such corruption. We introduce an approach motivated by very recent insights into median-of-means and Le Cam’s principle, we show that the approach can be readily implemented, and we demonstrate that it performs very well in practice. In conclusion, we believe that our approach is a very promising alternative to standard parameter training based on least-squares and cross-entropy loss.

1 Introduction

Deep learning is regularly used in safety-critical applications. For example, deep learning is used in the object-recognition systems of autonomous cars, where malfunction may lead to severe injury or death. It has been shown that data corruption can have dramatic effects on such critical deep-learning pipelines [1, 54, 20, 48, 42, 18, 21]. This insight has sparked research on robust deep learning based on, for example, adversarial training [34, 19, 36, 46, 41], sensitivity analysis [49], or noise correction [37, 53, 2].

Research on robust deep learning focuses usually on “adversarial attacks,” that is, intentional data corruptions designed to cause failures of specific pipelines. In contrast, the fact that data is often of poor quality much more generally has received little attention. But low-quality data is very common, simply because data used for deep learning is rarely collected based on rigid experimental designs but rather amassed from whatever resources are available [39, 9]. Among the few papers that consider such corruptions are [4, 5, 17, 50, 29], who replace the standard loss functions, such as squared error and soft-max cross entropy loss functions by some Lipschitz-continuous alternatives, such as Huber loss functions. But there is much room for improvement, especially because the existing methods do not make efficient use of the uncorrupted samples in the data.

In this paper, we devise a novel approach to deep learning with “randomly” corrupted data. The inspiration is the very recent line of research on median-of-means [32, 33, 28] and Le Cam’s procedure [22, 23] in linear regression [24, 25]. We especially mimic [25] in defining parameter updates in a min-max fashion. We show that this approach indeed outmatches other approaches on simulated and real-world data.

Our three main contributions are:

- We introduce a robust training scheme for neural networks that incorporates the median-of-means principle through Le Cam’s procedure.
- We show that our approach can be implemented by using a simple gradient-based algorithm.
- We demonstrate that our approach outperforms standard deep-learning pipeline across different levels of corruption.

Outline of the paper In Section 2, we state the problem and give a step-by-step derivation of the DeepMoM estimator (Definition 1). In Section 4, we highlight similarities and differences to other approaches. In Section 4.1, we establish a stochastic-gradient algorithm to compute our estimators (Algorithm 1). In Sections 4.2 and 4.3, we demonstrate that our approach rivals or outmatches traditional training schemes based on least-squares and on cross-entropy both for simulated corrupted and uncorrupted data. In Section 5, we demonstrate the same on real data. Finally, in Section 6, we summarize the results of this work and conclude.

2 Framework and estimator

We first introduce the statistical framework and our corresponding estimator. We consider data $(\mathbf{y}_1, \mathbf{x}_1), \dots, (\mathbf{y}_n, \mathbf{x}_n) \in \mathbb{R}^c \times \mathbb{R}^p$ with $c, p \in \{1, 2, \dots\}$ such that

$$\mathbf{y}_i = \mathbf{g}_*[\mathbf{x}_i] + \mathbf{u}_i \quad i \in \{1, \dots, n\}, \quad (1)$$

where $\mathbf{g}_* : \mathbb{R}^p \mapsto \mathbb{R}^c$ is the unknown data-generating function, and $\mathbf{u}_i \in \mathbb{R}^c$ are the stochastic error vectors. In particular, each \mathbf{x}_i is an input of the system and \mathbf{y}_i the corresponding output. The data is partitioned into two parts: the first part comprises the informative samples; the second part comprises the problematic samples (such as corrupted samples—irrespective of what the source of the corruption is). The two parts are index by $\mathcal{I} \subset \{1, \dots, n\}$ and $\mathcal{O} := \{1, \dots, n\} \setminus \mathcal{I}$, respectively. Of course, the sets \mathcal{I} and \mathcal{O} are unknown in practice (otherwise, one could simply remove the problematic samples). In brief, we consider a standard deep-learning setup—with the only exception that we make an explicit distinction between “good” and “bad” samples.

Our general goal is then, as usual, to approximate the data-generating function \mathbf{g}_* defined in (1). But our specific goal is to take into account the fact that there may be problematic samples. Our candidate functions are feed-forward neural networks $\mathbf{g}_{\mathbf{M}, \boldsymbol{\theta}}$ of the form

$$\mathbf{g}_{\mathbf{M}, \boldsymbol{\theta}}[\mathbf{x}] := M^l \mathbf{f}^l [M^{l-1} \dots \mathbf{f}^1 [M^0 \mathbf{x} + \boldsymbol{\theta}^0] + \boldsymbol{\theta}^{l-1}] + \boldsymbol{\theta}^l \quad \mathbf{x} \in \mathbb{R}^p, \quad (2)$$

indexed by the parameter spaces

$$\mathcal{M} := \left\{ \mathbf{M} = (M^0, \dots, M^l) : M^j \in \mathbb{R}^{p^{j+1} \times p^j} \text{ for all } j \in \{0, \dots, l\} \right\}$$

and

$$\boldsymbol{\Theta} := \left\{ \boldsymbol{\theta} = (\boldsymbol{\theta}^0, \dots, \boldsymbol{\theta}^l) : \boldsymbol{\theta}^j \in \mathbb{R}^{p^{j+1}} \text{ for all } j \in \{0, \dots, l\} \right\},$$

where l is the number of layers, $M^j \in \mathbb{R}^{p^{j+1} \times p^j}$ are the (finite-dimensional) weight matrices with $p^{l+1} = c$ and $p^0 = p$, $\boldsymbol{\theta}^j \in \mathbb{R}^{p^{j+1}}$ are bias parameters, and $\mathbf{f}^j : \mathbb{R}^{p^{j+1}} \rightarrow \mathbb{R}^{p^{j+1}}$ are the activation functions. For ease of exposition, we concentrate on ReLU activation, that is, $(\mathbf{f}^j[\mathbf{x}])_i := \max\{0, (\mathbf{x})_i\}$ for $\mathbf{x} \in \mathbb{R}^{p^{j+1}}$, $i \in \{1, \dots, p^{j+1}\}$, and $j \in \{1, \dots, l\}$ [30].

Neural networks, such as those in (2), are typically fitted to data by minimizing the sum of loss function: $\min_{\mathbf{M}, \boldsymbol{\theta}} \{\sum_{i=1}^n \mathcal{L}_{\mathbf{M}, \boldsymbol{\theta}}[\mathbf{y}_i, \mathbf{x}_i]\}$. The two standard loss functions for regression problems ($c = 1$) and classification problems ($c \in \{2, 3, \dots\}$) are the squared-error (SE) loss

$$\mathcal{L}_{\mathbf{M}, \boldsymbol{\theta}}^{\text{SE}}[\mathbf{y}_i, \mathbf{x}_i] := (\mathbf{y}_i - \mathbf{g}_{\mathbf{M}, \boldsymbol{\theta}}[\mathbf{x}_i])^2 \quad (3)$$

and the soft-max cross entropy (SCE) loss

$$\mathcal{L}_{\mathbf{M}, \boldsymbol{\theta}}^{\text{SCE}}[\mathbf{y}_i, \mathbf{x}_i] := -(\mathbf{y}_i)_j \log \left\{ \frac{\exp \{(\mathbf{g}_{\mathbf{M}, \boldsymbol{\theta}}[\mathbf{x}_i])_j\}}{\sum_{j=1}^c \exp \{(\mathbf{g}_{\mathbf{M}, \boldsymbol{\theta}}[\mathbf{x}_i])_j\}} \right\} \quad j \in \{1, \dots, c\}, \quad (4)$$

respectively. It is well known that such loss functions efficient on benign data but sensitive to heavy-tailed data, corrupted samples, and so forth [15].

We want to keep those loss functions' efficiency on benign samples, but, at the same time, avoid their failure in the presence of problematic samples. We achieve this by a median-of-means approach (MoM) inspired by [25]. The details of the MoM approach are mathematically intricate, but the general idea is simple. We thus describe the general idea first and then formally define the estimator afterward. The MoM approach can roughly be formulated in terms of three-step updates:

Step 1: Partition the data into blocks of samples.

Step 2: On each block, calculate the empirical mean of the loss increment with respect to two separate sets of parameters $(\mathbf{M}_1, \boldsymbol{\theta}_1), (\mathbf{M}_2, \boldsymbol{\theta}_2) \in (\mathcal{M}, \Theta)$ and the standard loss function ($\mathcal{L}_{\mathbf{M}, \boldsymbol{\theta}}^{\text{SE}}$ in regression and $\mathcal{L}_{\mathbf{M}, \boldsymbol{\theta}}^{\text{SCE}}$ in classification).

Step 3: Use the block that corresponds to the median of the empirical means in Step 2 to update the parameters.

Go back to Step 1 until convergence.

Let us now be more formal. In the first step, we consider $b \in \{1, \dots, n\}$ blocks $\mathcal{B}_1, \dots, \mathcal{B}_b \subset \{1, \dots, n\}$, that are an equipartition of $\{1, \dots, n\}$, which means the blocks have equal cardinalities $|\mathcal{B}_1| = \dots = |\mathcal{B}_b|$, that cover the entire index set $\cup_{k=1}^b \mathcal{B}_k = \{1, \dots, n\}$. In practice, we set $|\mathcal{B}_1| = \dots = |\mathcal{B}_{b-1}| = \lfloor n/b \rfloor$, where $\lfloor n/b \rfloor = \max\{a \in \{1, 2, \dots\} : a \leq n/b\}$ and $|\mathcal{B}_b| = n - \sum_{i=1}^{b-1} |\mathcal{B}_i|$, if b does not divide n .

Given $(\mathbf{M}_1, \boldsymbol{\theta}_1), (\mathbf{M}_2, \boldsymbol{\theta}_2) \in (\mathcal{M}, \Theta)$, the quantities in Step 2 is defined by

$$P_{\mathcal{B}_k}[(\mathbf{M}_1, \boldsymbol{\theta}_1), (\mathbf{M}_2, \boldsymbol{\theta}_2)] := \frac{1}{|\mathcal{B}_k|} \left[\sum_{i \in \mathcal{B}_k} \mathcal{L}_{\mathbf{M}_1, \boldsymbol{\theta}_1}[\mathbf{y}_i, \mathbf{x}_i] - \mathcal{L}_{\mathbf{M}_2, \boldsymbol{\theta}_2}[\mathbf{y}_i, \mathbf{x}_i] \right] \quad k \in \{1, \dots, b\}, \quad (5)$$

and we denote by $Q_{\mathcal{B}_1, \dots, \mathcal{B}_b}^{\alpha}[(\mathbf{M}_1, \boldsymbol{\theta}_1), (\mathbf{M}_2, \boldsymbol{\theta}_2)]$ an α -quantile of the set

$$\{P_{\mathcal{B}_1}[(\mathbf{M}_1, \boldsymbol{\theta}_1), (\mathbf{M}_2, \boldsymbol{\theta}_2)], \dots, P_{\mathcal{B}_b}[(\mathbf{M}_1, \boldsymbol{\theta}_1), (\mathbf{M}_2, \boldsymbol{\theta}_2)]\};$$

in particular, in Step 3, we compute the empirical median-of-means in Step 2 by defining

$$\begin{aligned} \text{MoM}_{\mathcal{B}_1, \dots, \mathcal{B}_b}[(\mathbf{M}_1, \boldsymbol{\theta}_1), (\mathbf{M}_2, \boldsymbol{\theta}_2)] := \\ \max_k \{P_{\mathcal{B}_k}[(\mathbf{M}_1, \boldsymbol{\theta}_1), (\mathbf{M}_2, \boldsymbol{\theta}_2)] : P_{\mathcal{B}_k}[(\mathbf{M}_1, \boldsymbol{\theta}_1), (\mathbf{M}_2, \boldsymbol{\theta}_2)] \leq Q_{\mathcal{B}_1, \dots, \mathcal{B}_b}^{1/2}[(\mathbf{M}_1, \boldsymbol{\theta}_1), (\mathbf{M}_2, \boldsymbol{\theta}_2)]\}. \end{aligned} \quad (6)$$

Our estimator is then the solution of the min-max problem of the increment tests defined in the following. (The estimator can also be seen as a generalization of the standard least-squares/cross-entropy approaches—see Appendix C.)

Definition 1 (DeepMoM). *For $b \in \{1, \dots, n\}$ and given blocks $\mathcal{B}_1, \dots, \mathcal{B}_b$ described in the above, we define*

$$\widehat{\mathbf{W}}_{\text{MoM}}^{\mathcal{B}_1, \dots, \mathcal{B}_b} := \arg \min_{(\mathbf{M}_1, \boldsymbol{\theta}_1) \in (\mathcal{M}, \Theta)} \sup_{(\mathbf{M}_2, \boldsymbol{\theta}_2) \in (\mathcal{M}, \Theta)} \text{MoM}_{\mathcal{B}_1, \dots, \mathcal{B}_b}[(\mathbf{M}_1, \boldsymbol{\theta}_1), (\mathbf{M}_2, \boldsymbol{\theta}_2)].$$

The rational is as follows: one the one hand, using least-squares/cross-entropy on each block ensures efficient use of the “good” samples; on the other hand, using the median over the blocks removes the corruptions and, therefore, ensures robustness toward the “bad” samples.

3 Related literature

We now take a moment to highlight relationships with other approaches as well as differences to those approaches. Since problematic samples are the rule rather than an exception in deep learning, the sensitivity of the standard loss functions has sparked much research interest. In regression settings, for example, [4, 5, 17, 50, 29] have replaced the squared-error loss by the absolute-deviation loss

$\mathcal{L}_{M,\theta}^{\text{AD}}[\mathbf{y}_i, \mathbf{x}_i] := |\mathbf{y}_i - \mathbf{g}_{M,\theta}[\mathbf{x}_i]|$, which generates estimators for the empirical median, or the Huber loss function [15, 16, 13]

$$\mathcal{L}_{M,\theta,k}^{\text{H}}[\mathbf{y}_i, \mathbf{x}_i] := \begin{cases} \frac{1}{2}(\mathbf{y}_i - \mathbf{g}_{M,\theta}[\mathbf{x}_i])^2 & |\mathbf{y}_i - \mathbf{g}_{M,\theta}[\mathbf{x}_i]| \leq k \\ k(|\mathbf{y}_i - \mathbf{g}_{M,\theta}[\mathbf{x}_i]| - \frac{1}{2}k); & |\mathbf{y}_i - \mathbf{g}_{M,\theta}[\mathbf{x}_i]| > k, \end{cases}$$

where $k \in (0, \infty)$ is a tuning parameter that determines the robustness of the function. In classification settings, for example, [11, 35, 51] have added an ℓ_1 penalty on the parameters. Changing the loss function in those ways can make the estimators robust toward the problematic data, but it also forfeits the efficiency of the standard loss functions in using the informative data. In contrast, our approach offers robustness with respect to the “bad” samples but also efficient use of the “good” samples.

Another related topic is adversarial attacks. Adversarial attacks are intentional corruptions of the data with the goal of exploiting weaknesses of specific deep-learning pipelines [21, 10, 6, 43, 3]. Hence, papers on adversarial attacks and our paper study data corruption. However, the perspectives on corruptions are very different: while the literature on adversarial attacks has a notion of a “mean-spirited opponent,” we have a much more general notion of “good” and “bad” samples. The adversarial-attack perspective is much more common in deep learning, but our view is much more common in the sciences more generally. The different notions also lead to different methods: methods in the context of adversarial attacks concern specific types of attacks and pipelines, while our method can be seen as a way to render deep learning more robust in general. A consequence of the different views is that adversarial attacks are designed for specific purposes, while our approach can be seen as a general way to make deep learning more robust in general. It would be misleading to include methods from the adversarial-attack literature in our numerical comparisons (they do not perform well simply because they are typically designed for very specific types of attacks and pipelines), but one could use our method in adversarial-attack frameworks. To avoid digression, we defer such studies to future work.

The following papers are related on a more general level: [14] highlights that the combination of non-robust methods does not lead to a robust method. [7] shows that even the detection of problematic input is very difficult. [52] introduces a notion of algorithmic robustness to study differences between training errors and expected errors. [45] states that an ensemble of two robust methods, each of which is robust to a different form of perturbation, may be robust to neither. [47] demonstrates that there exists a trade-off between a model’s standard accuracy and its robustness to adversarial perturbations.

4 Algorithm and numerical analysis

In this section, we devise an algorithm for computing the DeepMoM estimator of Definition 1. We then corroborate in simulations that our estimator is both robust toward corruptions as well as efficient in using benign data.

4.1 Algorithm

It turns out that MoM can be computed with standard optimization techniques. In particular, we can apply stochastic-gradient steps. The only minor challenge is that the estimator involves both a minimum and a supremum, but this can be addressed by using two updates in each optimization step: one update to make progress with respect to the minimum, and one update to make progress with respect to the supremum.

To be more formal, we want to compute the estimator $\widehat{\mathbf{W}}_{\text{MoM}}^{\mathcal{B}_1, \dots, \mathcal{B}_b}$ of Definition 1 for given blocks $\mathcal{B}_1, \dots, \mathcal{B}_b$ on data defined in Section 2. This amounts to finding updates such that our objective function

$$((\mathbf{M}_1, \boldsymbol{\theta}_1), (\mathbf{M}_2, \boldsymbol{\theta}_2)) \mapsto \text{MoM}_{\mathcal{B}_1, \dots, \mathcal{B}_b}[(\mathbf{M}_1, \boldsymbol{\theta}_1), (\mathbf{M}_2, \boldsymbol{\theta}_2)]$$

descents in its first arguments $(\mathbf{M}_1, \boldsymbol{\theta}_1)$ and ascents in its second arguments $(\mathbf{M}_2, \boldsymbol{\theta}_2)$. Hence, we are concerned with the gradients of

$$(\mathbf{M}_1, \boldsymbol{\theta}_1) \mapsto \text{MoM}_{\mathcal{B}_1, \dots, \mathcal{B}_b}[(\mathbf{M}_1, \boldsymbol{\theta}_1), (\mathbf{M}_2^0, \boldsymbol{\theta}_2^0)] \quad (7)$$

and

$$(\mathbf{M}_2, \boldsymbol{\theta}_2) \mapsto \text{MoM}_{\mathcal{B}_1, \dots, \mathcal{B}_b}[(\mathbf{M}_1^0, \boldsymbol{\theta}_1^0), (\mathbf{M}_2, \boldsymbol{\theta}_2)] \quad (8)$$

for fixed $(\mathbf{M}_1^0, \boldsymbol{\theta}_1^0), (\mathbf{M}_2^0, \boldsymbol{\theta}_2^0) \in (\mathcal{M}, \Theta)$.

For simplicity, the gradient of an objective function $f : (\mathbf{M}, \boldsymbol{\theta}) \mapsto f[(\mathbf{M}, \boldsymbol{\theta})]$ with respect to $(\mathbf{M}, \boldsymbol{\theta})$ at a point $(\mathbf{M}^0, \boldsymbol{\theta}^0)$ is denoted by $\nabla_{(\mathbf{M}, \boldsymbol{\theta})} f[(\mathbf{M}, \boldsymbol{\theta})]_{|(\mathbf{M}, \boldsymbol{\theta})=(\mathbf{M}^0, \boldsymbol{\theta}^0)}$, and the derivative of the activation functions \mathfrak{f}^j are denoted by $(\mathfrak{f}^j)'$. (In line with the usual conventions, the derivative of the ReLU function at zero is set to zero.)

The computation of the gradients of (7) and (8) are deferred to the Appendix A.

The above computations are then the basis for our computation of $\widehat{\mathbf{W}}_{\text{MoM}}^{\mathcal{B}_1, \dots, \mathcal{B}_b}$ in Algorithm 1. In that algorithm, we set

$$\|(\mathbf{M}_1, \boldsymbol{\theta}_1) - (\mathbf{M}_2, \boldsymbol{\theta}_2)\|_2 := \sqrt{\sum_{j=0}^l \sum_{v=1}^{p^{j+1}} \sum_{w=1}^{p^j} ([M_1^j - M_2^j]_{v,w})^2 + \sum_{j=0}^l \sum_{v=1}^{p^{j+1}} ([\theta_1^j - \theta_2^j]_v)^2}$$

for $(\mathbf{M}_1, \boldsymbol{\theta}_1), (\mathbf{M}_2, \boldsymbol{\theta}_2) \in (\mathcal{M}, \Theta)$.

Input: data $(\mathbf{y}_1, \mathbf{x}_1), \dots, (\mathbf{y}_n, \mathbf{x}_n)$, number of blocks b , initial parameters $(\mathbf{M}_1^0, \boldsymbol{\theta}_1^0), (\mathbf{M}_2^0, \boldsymbol{\theta}_2^0)$, iteration number i_{\max} , stopping criterion d , batch size h , and learning rate r .

Output: $\widehat{\mathbf{W}}_{\text{MoM}}^{\mathcal{B}_1, \dots, \mathcal{B}_b}$ of Definition 1.

while $i \leq i_{\max}$ **do**

 1. Randomly select a batch of h data points.

 2. Generate blocks $\mathcal{B}_1, \dots, \mathcal{B}_b$ for the selected data.

 3. Update gradients for the first arguments :

$$(\mathbf{M}_1^{i+1}, \boldsymbol{\theta}_1^{i+1}) := (\mathbf{M}_1^i, \boldsymbol{\theta}_1^i) - r \nabla_{\mathbf{M}_1, \boldsymbol{\theta}_1} \text{MoM}_{\mathcal{B}_1, \dots, \mathcal{B}_b}[(\mathbf{M}_1, \boldsymbol{\theta}_1), (\mathbf{M}_2^i, \boldsymbol{\theta}_2^i)]_{|(\mathbf{M}_1, \boldsymbol{\theta}_1)=(\mathbf{M}_1^i, \boldsymbol{\theta}_1^i)}$$

 4. First stopping criterion:

if $\|(\mathbf{M}_1^{i+1}, \boldsymbol{\theta}_1^{i+1}) - (\mathbf{M}_1^i, \boldsymbol{\theta}_1^i)\|_2 \leq d$ **then**

break

end if

 5. Update gradients for the second arguments :

$$(\mathbf{M}_2^{i+1}, \boldsymbol{\theta}_2^{i+1}) := (\mathbf{M}_2^i, \boldsymbol{\theta}_2^i) - r \nabla_{\mathbf{M}_2, \boldsymbol{\theta}_2} \text{MoM}_{\mathcal{B}_1, \dots, \mathcal{B}_b}[(\mathbf{M}_1^{i+1}, \boldsymbol{\theta}_1^{i+1}), (\mathbf{M}_2, \boldsymbol{\theta}_2)]_{|(\mathbf{M}_2, \boldsymbol{\theta}_2)=(\mathbf{M}_2^i, \boldsymbol{\theta}_2^i)}$$

 6. Second stopping criterion:

if $\|(\mathbf{M}_2^{i+1}, \boldsymbol{\theta}_2^{i+1}) - (\mathbf{M}_2^i, \boldsymbol{\theta}_2^i)\|_2 \leq d$ **then**

break

end if

end while

Algorithm 1: stochastic gradient-based algorithm for DeepMoM

Throughout the paper, the batch size is $h = 250$, maximum number of iteration $i_{\max} = 10^6$, and the stopping criterion $d = 10^{-3}$.

Algorithm 1 provides a stochastic approximation method for standard gradient-descent optimization of the empirical-median-of-means function formulated in Display (6). A mathematical result on the convergence of the algorithm is provided in the Appendix B.

4.2 Numerical analysis for regression data

We now consider the regression data and show that our MoM approach can indeed outmatch other approaches, such as vanilla squared-error, absolute-deviation, and Huber estimation.

General setup We consider a uniform width $\bar{p} := p^1 = \dots = p^l$. The elements of the input vectors $\mathbf{x}_1, \dots, \mathbf{x}_n$ are i.i.d. sampled from a standard Gaussian distribution and then normalized such that $\sum_{i=1}^n ((\mathbf{x}_i)_j)^2 = 1$ for all $j \in \{1, \dots, p\}$. The elements of the true weight matrices $\mathbf{M}^* = (M^0, \dots, M^l)$ and true bias parameters $\boldsymbol{\theta}^* = (\theta^0, \dots, \theta^l)$ are i.i.d. sampled from a uniform distribution on $[-1, 1]$. The stochastic noise variables $\mathbf{u}_1, \dots, \mathbf{u}_n$ are i.i.d. sampled from a centered Gaussian distribution such that the empirical signal to noise ratio equals 10.

Data corruptions We corrupt the data in three different ways. Recall that \mathcal{I} and \mathcal{O} denote the sets of informative samples and corrupted samples (outliers), respectively.

Corrupted outputs (outliers): The noise variables \mathbf{u}_i for outliers $i \in \mathcal{O}$ are replaced by i.i.d. samples from a uniform distribution on $[3 \max_i |\mathbf{g}_{M^*, \theta^*}(\mathbf{x}_i)|, 5 \max_i |\mathbf{g}_{M^*, \theta^*}(\mathbf{x}_i)|]$. This means that the corresponding outputs \mathbf{y}_i are subject to heavy yet bounded corruptions.

Corrupted outputs (everywhere): All noise variables are replaced by i.i.d. samples from a Student's t-distribution with df degrees of freedom. This means that all outputs \mathbf{y}_i are subject to unbounded corruptions.

Corrupted inputs: The elements of the input vectors \mathbf{x}_i for outliers $i \in \mathcal{O}$ receive (after computing \mathbf{y}_i) an additional perturbation that is i.i.d. sampled from a standard Gaussian distribution. This means that the analyst gets to see corrupted versions of the input.

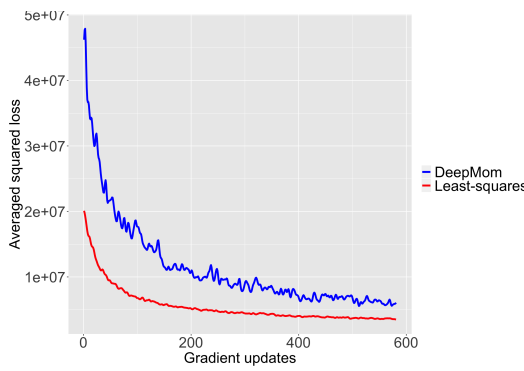


Figure 1: a comparison of the averaged squared loss of least-squares and DeepMoM (as in Algorithm 1) with $(n, p, l, \bar{p}) = (2000, 50, 7, 30)$, $|\mathcal{I}|/n = 0.75$, and $b = 21$ as a function of the gradient updates

Table 2: MoM_{min} outperforms \widehat{W}_{SE} , \widehat{W}_{AD} , and Huber_{min} in robustness for all settings.

$(n, p, l, \bar{p}) = (1600, 50, 10, 20)$				
Corrupted outputs (uniform distribution)				
Scaled mean of prediction errors				
$ \mathcal{I} /n$	MoM _{min}	AD	Huber _{min}	SE
100%	1.00	2.04	1.71	3.62
95%	1.58	19.85	10.66	31.66
85%	1.73	63.69	70.71	116.85
75%	2.06	159.17	133.71	229.14

Corrupted outputs (t-distribution)				
Scaled mean of prediction errors				
df	MoM _{min}	AD	Huber _{min}	SE
10	1.05	1.72	1.75	2.83
1	1.99	2.18	1.81	3.93

Corrupted inputs				
Scaled mean of prediction errors				
$ \mathcal{I} /n$	MoM _{min}	AD	Huber _{min}	SE
95%	1.63	2.37	1.97	2.70
85%	1.75	2.08	2.53	3.21
75%	1.86	2.22	2.63	3.78

Table 1: MoM_{min} outperforms \widehat{W}_{SE} , \widehat{W}_{AD} , and Huber_{min} in robustness for all settings.

$(n, p, l, \bar{p}) = (1000, 50, 5, 50)$				
Corrupted outputs (uniform distribution)				
Scaled mean of prediction errors				
$ \mathcal{I} /n$	MoM _{min}	AD	Huber _{min}	SE
100%	1.00	1.58	1.29	1.60
95%	1.22	12.09	7.36	17.42
85%	1.48	26.81	33.69	72.21
75%	2.47	80.34	68.76	121.58

Corrupted outputs (t-distribution)				
Scaled mean of prediction errors				
df	MoM _{min}	AD	Huber _{min}	SE
10	1.16	1.40	1.34	1.93
1	1.11	1.38	1.32	1.83

Corrupted inputs				
Scaled mean of prediction errors				
$ \mathcal{I} /n$	MoM _{min}	AD	Huber _{min}	SE
95%	1.26	1.46	1.77	1.61
85%	1.27	1.38	1.38	1.80
75%	1.37	1.66	1.90	1.75

Table 3: MoM_{min} outperforms \widehat{W}_{SE} , \widehat{W}_{AD} , and Huber_{min} in robustness for all settings.

$(n, p, l, \bar{p}) = (2000, 50, 7, 30)$				
Corrupted outputs (uniform distribution)				
Scaled mean of prediction errors				
$ \mathcal{I} /n$	MoM _{min}	AD	Huber _{min}	SE
100%	1.00	1.74	1.53	2.05
95%	1.05	14.34	10.84	14.45
85%	1.39	44.80	44.29	44.58
75%	1.95	78.19	95.02	82.56

Corrupted outputs (t-distribution)				
Scaled mean of prediction errors				
df	MoM _{min}	AD	Huber _{min}	SE
10	0.97	1.58	1.70	2.44
1	0.99	1.68	1.78	2.05

Corrupted inputs				
Scaled mean of prediction errors				
$ \mathcal{I} /n$	MoM _{min}	AD	Huber _{min}	SE
95%	1.01	1.60	1.76	1.99
85%	1.07	1.66	1.58	1.87
75%	1.13	1.58	1.38	2.13

Error quantification 20 data sets are generated as described above. The first half of the samples in each data set are assigned to training and the remaining half of the samples to testing. For each estimator $\widehat{\mathbf{W}}$, the average of the generalization error $2/n \sum_{i=\frac{n}{2}+1}^n (\mathbf{g}_{\mathbf{M}^*, \boldsymbol{\theta}^*}[\mathbf{x}_i] - \mathbf{g}_{\widehat{\mathbf{W}}}[\mathbf{x}_i])^2$ is computed and re-scaled with respect to the MoM approach with 100% informative data.

The contenders are MoM, absolute error, Huber, and the squared error loss functions. For convenience, we denote $\widehat{\mathbf{W}}_{\text{SE}}$, $\widehat{\mathbf{W}}_{\text{AD}}$, and $\widehat{\mathbf{W}}_{\text{H}}^k$ as the estimators obtained by minimizing $2 \sum_{i=1}^n \mathcal{L}_{\mathbf{M}, \boldsymbol{\theta}}^{\text{SE}}[\mathbf{y}_i, \mathbf{x}_i]/n$, $2 \sum_{i=1}^n \mathcal{L}_{\mathbf{M}, \boldsymbol{\theta}}^{\text{AD}}[\mathbf{y}_i, \mathbf{x}_i]/n$, and $2 \sum_{i=1}^n \mathcal{L}_{\mathbf{M}, \boldsymbol{\theta}, k}^{\text{H}}[\mathbf{y}_i, \mathbf{x}_i]/n$ on training data, respectively.

Besides, we consider a sequence of MoM estimators $\widehat{\mathbf{W}}_{\text{MoM}}^{\mathcal{B}_1, \dots, \mathcal{B}_b}$, where $b \in \{1, 21, \dots, 121\}$, and we define MoM_{\min} as

$$\text{MoM}_{\min} := \min_b \left\{ \frac{2}{n} \sum_{i=\frac{n}{2}+1}^n (\mathbf{g}_{\mathbf{M}^*, \boldsymbol{\theta}^*}[\mathbf{x}_i] - \mathbf{g}_{\widehat{\mathbf{W}}_{\text{MoM}}^{\mathcal{B}_1, \dots, \mathcal{B}_b}}[\mathbf{x}_i])^2 \right\}.$$

We further consider a sequence of Huber estimators $\widehat{\mathbf{W}}_{\text{H}}^{k_q}$, where k_q are the q -th quantile of $\{|\mathbf{y}_i|\}_{i \in \{1, \dots, n\}}$ with $q \in \{75, 80, 85, 90, 95, 100\}$, and we define Huber_{\min} as

$$\text{Huber}_{\min} := \min_q \left\{ \frac{2}{n} \sum_{i=\frac{n}{2}+1}^n (\mathbf{g}_{\mathbf{M}^*, \boldsymbol{\theta}^*}[\mathbf{x}_i] - \mathbf{g}_{\widehat{\mathbf{W}}_{\text{H}}^{k_q}}[\mathbf{x}_i])^2 \right\}.$$

Results and conclusions The results for different settings are summarized in Tables 1–3. First, we observe that MoM, least-squares, and Huber estimators behave very similarly in the uncorrupted case ($|\mathcal{I}|/n = 100\%$) and for mildly corrupted outputs ($df = 10$). But once the corruptions are more substantial, our MoM approach clearly outperforms the other approaches. In general, we conclude that MoM is efficient on benign data and robust on problematic data.

4.3 Numerical analysis for classification data

We now consider the multi-class problems and demonstrate that the DeepMoM estimator in Definition 1 outperforms the soft-max cross-entropy estimation in terms of prediction accuracies.

General setup We consider a spiral data set with $(n, p) = (1000, 2)$ consisting of five classes $\mathcal{C}_1, \dots, \mathcal{C}_5$ with identical cardinalities $|\mathcal{C}_1| = \dots = |\mathcal{C}_5| = 200$ that span the entire index set $\bigcup_{j=1}^5 \mathcal{C}_j = \{1, \dots, n\}$. We denote the symbol \circ as the Hadamard product between two vectors and $\mathcal{N}(\mu, \sigma^2)$ as the normal distribution with mean μ and standard deviation σ . For each class $j \in \{1, \dots, 5\}$, we have

$$(\mathbf{y}_i)_k := \begin{cases} 1 & k = j \\ 0 & k \neq j \end{cases} \quad k \in \{1, \dots, 5\}, \quad i \in \mathcal{C}_j,$$

$((\mathbf{x}_i)_1)_{i \in \mathcal{C}_j} := \mathbf{r} \circ \sin(\mathbf{t})$, and $((\mathbf{x}_i)_2)_{i \in \mathcal{C}_j} := \mathbf{r} \circ \cos(\mathbf{t})$, where the elements of \mathbf{r} and \mathbf{t} are given by $(\mathbf{r})_m := 0.05 + (1 - 0.05)(m - 1)/200$ and $(\mathbf{t})_m := (j - 1)3.7 + 3.7(m - 1)/200 + \epsilon_m$ for $\epsilon_m \sim \mathcal{N}[0, 0.25]$ and $m \in \{1, \dots, 200\}$. The data is visualized in Figure 2.

To fit this data, we consider a two layers ReLU network with uniform width $\bar{p} := p^1 = p^2 = 150$. Each element of the input vectors $\mathbf{x}_1, \dots, \mathbf{x}_n$ are then divided by the maximum among them such that $\max_{i,j} (\mathbf{x}_i)_j = 1$ for all $i \in \{1, \dots, n/2\}$ and $j \in \{1, 2\}$.

Data corruptions We corrupt the spiral data using the two methods mentioned below.

Corrupted labels: The problematic labels \mathbf{y}_i for $i \in \mathcal{O}$ are shuffled to other class labels.

Corrupted inputs: The elements of the input vectors \mathbf{x}_i for outliers $i \in \mathcal{O}$ are subjected to an additional perturbation, as prescribed under Section 4.2.

Error quantification The first half of the samples will be used for training, while the other half will be used for testing. For the SCE estimator $\widehat{\mathbf{W}}_{\text{SCE}}$, which is computed by minimizing the

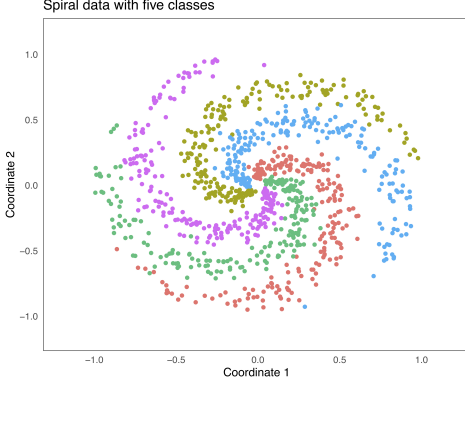


Figure 2: the two-dimensional spiral data set with five classes

mean of $\mathcal{L}_{M,\theta}^{\text{SCE}}[\mathbf{y}_i, \mathbf{x}_i]$ on training data, the generalization accuracy $2 \sum_{i=n/2+1}^n \mathbb{1}_{(\mathbf{y}_i = \mathbf{g}_{\widehat{\mathbf{W}}_{\text{SCE}}}[\mathbf{x}_i])}/n$ is calculated, where $\mathbb{1} : \mathbb{R}^c \mapsto \mathbb{R}$ is the indicator function defined by

$$\mathbb{1}_{(\mathbf{y}_i = \mathbf{g}_{\widehat{\mathbf{W}}_{\text{SCE}}}[\mathbf{x}_i])} := \begin{cases} 1 & \mathbf{y}_i = \mathbf{g}_{\widehat{\mathbf{W}}_{\text{SCE}}}[\mathbf{x}_i] \\ 0 & \mathbf{y}_i \neq \mathbf{g}_{\widehat{\mathbf{W}}_{\text{SCE}}}[\mathbf{x}_i] \quad i \in \{\frac{n}{2}, \dots, n\}. \end{cases}$$

We define the quantity MoM_{\min} as in Section 4.2 with the considered number of blocks $b \in \{1, 3, \dots, 11\}$.

Results and conclusions Table 4 summarizes the results for various settings. To begin, we see that DeepMoM and SCE estimators behave very closely in the uncorrupted and slightly corrupted labels ($|\mathcal{I}|/n = 100\%, 95\%$) and slightly corrupted inputs ($|\mathcal{I}|/n = 95\%, 85\%$) cases. However, when the corruptions are more serious, our DeepMoM estimator clearly outperforms the other approaches. In general, we conclude that MoM is efficient on benign data and robust on problematic data.

5 Applications

We now illustrate the potential of DeepMoM in practice. We demonstrate that DeepMoM can withstand data corruptions considerably better than usual approaches.

Application in regression data The first application is the prediction of the critical temperature of a superconductor. Superconductor materials have a wide range of practical uses. Because of their frictionless property, superconducting wires and electrical systems, for example, have the potential to transport and deliver electricity without any energy loss in the energy industry. This frictionless property, however, occurs only when the ambient temperature is at or below the critical temperature of the superconductor. As a result, the estimation of a superconductor's critical temperature has baffled scientists since the discovery of superconductivity.

The data [12, 8] contains $n = 21\,263$ samples and $p = 81$ features extracted from the superconductor's chemical formula [12]. In this example, we first select 15 000 samples randomly for training and keep the remaining 6 263 samples for testing. The normalization of the input data are the same as we described in Section 4.2. We fit this data by considering a two layers ReLU network with 50 neurons in the first hidden layer and 5 neurons in the second one.

Table 4: MoM_{\min} outperforms $\widehat{\mathbf{W}}_{\text{SCE}}$ in robustness for all settings

Corrupted outputs (shuffled labels)		
	Prediction accuracies	
$ \mathcal{I} /n$	MoM_{\min}	SCE
100%	95.6%	95.6%
95%	95.2%	94.2%
85%	88.0%	79.6%
75%	85.6%	73.2%

Corrupted inputs		
	Prediction accuracies	
$ \mathcal{I} /n$	MoM_{\min}	SCE
95%	95.6%	95.6%
85%	95.6%	95.6%
75%	93.8%	90.2%

Table 5: MoM_{min} outperforms its contenders in robustness for all settings

(a) Superconductor data set

Corrupted outputs: uniform distribution				
Scaled mean of prediction errors				
$ \mathcal{I} /n$	MoM _{min}	AD	Huber _{min}	SE
100%	1.00	3.47	1.02	1.00
95%	1.33	7.11	1.43	3.42
85%	1.37	11.34	1.79	17.29
75%	1.30	12.01	2.84	46.08

Corrupted outputs: t-distribution				
Scaled mean of prediction errors				
df	MoM _{min}	AD	Huber _{min}	SE
10	1.25	7.21	1.42	1.20
1	1.36	7.82	1.20	1.32

Corrupted inputs				
Scaled mean of prediction errors				
$ \mathcal{I} /n$	MoM _{min}	AD	Huber _{min}	SE
95%	1.19	2.41	1.13	1.10
85%	1.13	4.47	1.28	1.12
75%	1.49	7.53	1.41	1.41

(b) MNIST data set

Corrupted outputs (shuffled labels)		
Prediction accuracies		
$ \mathcal{I} /n$	MoM _{min}	SCE
100%	96.98%	96.98%
95%	96.62%	95.23%
85%	96.19%	85.27%
75%	94.54%	74.16%

Corrupted inputs		
Prediction accuracies		
$ \mathcal{I} /n$	MoM _{min}	SCE
95%	96.62%	96.62%
85%	96.62%	96.62%
75%	96.56%	96.56%

Application in classification data The second application is the classification of handwritten digit images for the values within $\{0, \dots, 9\}$ from the well-known MNIST data set [26, 27].

This data contains $n = 60\,000$ samples for training, $10\,000$ samples for testing, and $p = 784$ pixels as features. The preprocessing of the input data and the network settings are the same as we described in Section 4.2.

Our aim for these two types of applications is to validate the DeepMoM method on original data with some corruptions and compare the results to other robust competitors for deep learning, as specified in Section 4.2 and Section 4.3, respectively.

The predicted results of these two applications are presented in Table 5a and 5b, respectively. These results again suggest that DeepMoM estimator provides higher accuracies than its contenders.

6 Discussion

Our new approach to training the parameters of neural networks is robust against corrupted samples and yet leverages informative samples efficiently. We have confirmed these properties numerically in Sections 4.2, 4.3, and 5. The approach can, therefore, be used as a general substitute for basic least-squares-type or cross-entropy-type approaches.

We have restricted ourselves to feed-forward neural networks with ReLU activation, but there are no obstacles for applying our approach more generally, for example, to convolutional networks or other activation functions. However, to keep the paper clear and concise, we defer a detailed analysis of MoM in other deep-learning frameworks to future work.

Similarly, we model corruption by uniform or heavy-tailed random perturbations of the inputs or outputs or by randomly swapping labels, but, of course, one can conceive a plethora of different ways to corrupt data.

In sum, given modern data’s limitations and our approach’s ability to make efficient use of such data, we believe that our contribution can have a substantial impact on deep-learning practice.

Acknowledgments

We thank Guillaume Lecué, Timothé Mathieu, Mahsa Taheri, and Fang Xie for their insightful inputs and suggestions.

References

- [1] N. Akhtar and A. Mian. Threat of adversarial attacks on deep learning in computer vision: a survey. *arXiv:1801.00553*, 2018.
- [2] E. Arazo, D. Ortego, P. Albert, N. O'Connor, and K. McGuinness. Unsupervised label noise modeling and loss correction. *Proceedings of the 36th international conference on machine learning*, 97:312–321, 2019.
- [3] A. Athalye, L. Engstrom, A. Ilyas, and K. Kwok. Synthesizing robust adversarial examples. *arXiv:1707.07397*, 2018.
- [4] J. Barron. A general and adaptive robust loss function. *arXiv:1701.03077*, 2019.
- [5] V. Belagiannis, C. Rupprecht, G. Carneiro, and N. Navab. Robust optimization for deep regression. *arXiv:1505.06606*, 2015.
- [6] M. Brückner, C. Kanzow, and T. Scheffer. Static prediction games for adversarial learning problems. *Journal of machine learning research*, 13(85):2617–2654, 2012.
- [7] N. Carlini and D. Wagner. Adversarial examples are not easily detected: bypassing ten detection methods. *arXiv:1705.07263*, 2017.
- [8] D. Dua and C. Graff. UCI machine learning repository. *University of California, Irvine, School of Information and Computer Sciences*, 2017.
- [9] S. Friedrich, G. Antes, S. Behr, H. Binder, W. Brannath, F. Dumpert, K. Ickstadt, H. Kestler, J. Lederer, H. Leitgöb, M. Pauly, A. Steland, A. Wilhelm, and T. Friede. Is there a role for statistics in artificial intelligence? *arXiv:2009.09070*, 2020.
- [10] I. Goodfellow, P. McDaniel, and N. Papernot. Making machine learning robust against adversarial inputs : such inputs distort how machine-learning based systems are able to function in the world as it is. *Communications of the ACM*, 61(7):56–66, 2018.
- [11] I. Goodfellow, J. Shlens, and C. Szegedy. Explaining and harnessing adversarial examples. *arXiv:1412.6572*, 2015.
- [12] K. Hamidieh. A data-driven statistical model for predicting the critical temperature of a superconductor. *Computational materials science*, 154:346–354, 2018.
- [13] F. Hampel, E. Ronchetti, P. Rousseeuw, and W. Stahel. *Robust statistics: the approach based on influence functions*. Wiley, 2011.
- [14] W. He, J. Wei, X. Chen, N. Carlini, and D. Song. Adversarial example defenses: ensembles of weak defenses are not strong. *arXiv:1706.04701*, 2017.
- [15] P. Huber. Robust estimation of a location parameter. *Annals of mathematical statistics*, 35(1):73–101, 1964.
- [16] P. Huber and E. Ronchetti. *Robust statistics*. Wiley, 2009.
- [17] L. Jiang, Z. Zhou, T. Leung, L.-J. Li, and F.-F. Li. Mentornet: learning data-driven curriculum for very deep neural networks on corrupted labels. *arXiv:1712.05055*, 2018.
- [18] Tencent keen security lab. Experimental security research of tesla autopilot. *Tencent keen security lab*, 2019.
- [19] J. Kos and D. Song. Delving into adversarial attacks on deep policies. *arXiv:1705.06452*, 2017.
- [20] A. Kurakin, I. Goodfellow, and S. Bengio. Adversarial examples in the physical world. *arXiv:1607.02533*, 2016.
- [21] A. Kurakin, I. Goodfellow, and S. Bengio. Adversarial machine learning at scale. *arXiv:1611.01236*, 2016.
- [22] L. Le Cam. Convergence of estimates under dimensionality restrictions. *The annals of statistics*, 1(1):38–53, 1973.
- [23] L. Le Cam. Sums of independent random variables. *Asymptotic methods in statistical decision theory* *springer series in statistics*, page 399–456, 1986.
- [24] G. Lecué and M. Lerasle. Learning from mom's principles: Le cam's approach. *arXiv:1701.01961*, 2017.

[25] G. Lecué and M. Lerasle. Robust machine learning by median-of-means : theory and practice. *arXiv:1711.10306*, 2017.

[26] Y. LeCun, L. Bottou, Y. Bengio, and P. Haffner. Gradient-based learning applied to document recognition. *Proceedings of the IEEE*, 1998.

[27] Y. Lecun, C. Cortes, and C. Burges. The MNIST database. *MNIST handwritten digit database*.

[28] G. Lecué, M. Lerasle, and T. Mathieu. Robust classification via MOM minimization. *Machine learning*, 109(8):1635–1665, 2020.

[29] J. Lederer. Risk bounds for robust deep learning. *arXiv:2009.06202*, 2020.

[30] J. Lederer. Activation functions in artificial neural networks: a systematic overview. *arXiv:2101.09957*, 2021.

[31] C. Liu and M. Belkin. Accelerating SGD with momentum for over-parameterized learning. *arXiv:1810.13395*, 2019.

[32] G. Lugosi and S. Mendelson. Regularization, sparse recovery, and median-of-means tournaments. *Bernoulli*, 25(3), 2019.

[33] G. Lugosi and S. Mendelson. Risk minimization by median-of-means tournaments. *Journal of the European mathematical society*, 22(3):925–965, 2019.

[34] A. Madry, A. Makelov, L. Schmidt, D. Tsipras, and A. Vladu. Towards deep learning models resistant to adversarial attacks. *arXiv:1706.06083*, 2017.

[35] A. Madry, A. Makelov, L. Schmidt, D. Tsipras, and A. Vladu. Towards deep learning models resistant to adversarial attacks. *arXiv:1706.06083*, 2019.

[36] N. Papernot, P. McDaniel, X. Wu, S. Jha, and A. Swami. Distillation as a defense to adversarial perturbations against deep neural networks. *arXiv:1511.04508*, 2015.

[37] G. Patrini, A. Rozza, A. Menon, R. Nock, and L. Qu. Making deep neural networks robust to label noise: a loss correction approach. *arXiv*, 2017.

[38] R core team. R: a language and environment for statistical computing. *R Foundation for Statistical Computing*, 2017.

[39] Y. Roh, G. Heo, and S. Whang. A survey on data collection for machine learning: a big data - AI integration perspective. *IEEE transactions on knowledge and data engineering*, 33(4):1328–1347, 2021.

[40] D. Rumelhart, G. Hinton, and R. Williams. Learning representations by back-propagating errors. *Nature*, 323(6088):533–536, 1986.

[41] H. Salman, G. Yang, J. Li, P. Zhang, H. Zhang, I. Razenshteyn, and S. Bubeck. Provably robust deep learning via adversarially trained smoothed classifiers. *arXiv:1906.04584*, 2019.

[42] M. Sharif, S. Bhagavatula, L. Bauer, and M. Reiter. *Accessorize to a crime: real and stealthy attacks on state-of-the-art face recognition*. Proceedings of the 2016 ACM SIGSAC conference on computer and communications security, 2016.

[43] J. Su, D. Vargas, and K. Sakurai. One pixel attack for fooling deep neural networks. *IEEE transactions on evolutionary computation*, 23(5):828–841, 2019.

[44] R. Sun. Optimization for deep learning:theory and algorithms. *arXiv:1912.08957*, 2019.

[45] F. Tramèr and D. Boneh. Adversarial training and robustness for multiple perturbations. *arXiv:1904.13000*, 2019.

[46] F. Tramèr, A. Kurakin, N. Papernot, I. Goodfellow, D. Boneh, and P. McDaniel. Ensemble adversarial training: attacks and defenses. *arXiv:1705.07204*, 2017.

[47] D. Tsipras, S. Santurkar, L. Engstrom, A. Turner, and A. Madry. Robustness may be at odds with accuracy, 2019.

[48] H. Wang and C.-N. Yu. A direct approach to robust deep learning using adversarial networks. *arXiv:1905.09591*, 2019.

[49] T. Wang, Y. Gu, D. Mehta, X. Zhao, and E. Bernal. Towards robust deep neural networks. *arXiv:1810.11726*, 2018.

[50] Z. Wang, S. Chang, Y. Yang, D. Liu, and T. Huang. Studying very low resolution recognition using deep networks. *arXiv:1601.04153*, 2016.

- [51] E. Wong and J. Kolter. Provable defenses against adversarial examples via the convex outer adversarial polytope. *arXiv:1711.00851*, 2018.
- [52] H. Xu and S. Mannor. Robustness and generalization. *arXiv:1005.2243*, 2010.
- [53] K. Yi and J. Wu. Probabilistic end-to-end noise correction for learning with noisy labels. In *Proceedings of the IEEE/CVF conference on computer vision and pattern recognition*, 2019.
- [54] X. Yuan, P. He, Q. Zhu, and X. Li. Adversarial examples: attacks and defenses for deep learning. *IEEE transactions on neural networks and learning systems*, 30(9):2805–2824, 2019.

A Gradients

Given $(\mathbf{M}_1^0, \boldsymbol{\theta}_1^0), (\mathbf{M}_2^0, \boldsymbol{\theta}_2^0) \in (\mathcal{M}, \Theta)$, we can find—see the definition of the empirical median-of-means in (6)—indexes $k_1, k_2 \in \{1, \dots, b\}$ (which depend on $(\mathbf{M}_1, \boldsymbol{\theta}_1), (\mathbf{M}_2, \boldsymbol{\theta}_2) \in (\mathcal{M}, \Theta)$, respectively) such that $P_{\mathcal{B}_{k_1}}[(\mathbf{M}_1, \boldsymbol{\theta}_1), (\mathbf{M}_2^0, \boldsymbol{\theta}_2^0)] = \text{MoM}_{\mathcal{B}_1, \dots, \mathcal{B}_b}[(\mathbf{M}_1, \boldsymbol{\theta}_1), (\mathbf{M}_2^0, \boldsymbol{\theta}_2^0)]$ and $P_{\mathcal{B}_{k_2}}[(\mathbf{M}_1^0, \boldsymbol{\theta}_1^0), (\mathbf{M}_2, \boldsymbol{\theta}_2)] = \text{MoM}_{\mathcal{B}_1, \dots, \mathcal{B}_b}[(\mathbf{M}_1^0, \boldsymbol{\theta}_1^0), (\mathbf{M}_2, \boldsymbol{\theta}_2)]$.

Therefore, given $(\mathbf{M}_{11}^0, \boldsymbol{\theta}_{11}^0), (\mathbf{M}_{22}^0, \boldsymbol{\theta}_{22}^0) \in (\mathcal{M}, \Theta)$, the gradients of (7) and (8) defined in Section 4.1 are

$$\begin{aligned} & \nabla_{\mathbf{M}_1, \boldsymbol{\theta}_1} \text{MoM}_{\mathcal{B}_1, \dots, \mathcal{B}_b}[(\mathbf{M}_1, \boldsymbol{\theta}_1), (\mathbf{M}_2^0, \boldsymbol{\theta}_2^0)]|_{(\mathbf{M}_1, \boldsymbol{\theta}_1) = (\mathbf{M}_{11}^0, \boldsymbol{\theta}_{11}^0)} \\ &= \frac{1}{|\mathcal{B}_{k_1}|} \sum_{i \in \mathcal{B}_{k_1}} \nabla_{\mathbf{M}_1, \boldsymbol{\theta}_1} (\mathcal{L}_{\mathbf{M}_1, \boldsymbol{\theta}_1}[\mathbf{y}_i, \mathbf{x}_i] - \mathcal{L}_{\mathbf{M}_2^0, \boldsymbol{\theta}_2^0}[\mathbf{y}_i, \mathbf{x}_i])|_{(\mathbf{M}_1, \boldsymbol{\theta}_1) = (\mathbf{M}_{11}^0, \boldsymbol{\theta}_{11}^0)} \\ &= \frac{1}{|\mathcal{B}_{k_1}|} \sum_{i \in \mathcal{B}_{k_1}} \nabla_{\mathbf{M}_1, \boldsymbol{\theta}_1} \mathcal{L}_{\mathbf{M}_1, \boldsymbol{\theta}_1}[\mathbf{y}_i, \mathbf{x}_i]|_{(\mathbf{M}_1, \boldsymbol{\theta}_1) = (\mathbf{M}_{11}^0, \boldsymbol{\theta}_{11}^0)} \end{aligned}$$

and

$$\begin{aligned} & \nabla_{\mathbf{M}_2, \boldsymbol{\theta}_2} \text{MoM}_{\mathcal{B}_1, \dots, \mathcal{B}_b}[(\mathbf{M}_1^0, \boldsymbol{\theta}_1^0), (\mathbf{M}_2, \boldsymbol{\theta}_2)]|_{(\mathbf{M}_2, \boldsymbol{\theta}_2) = (\mathbf{M}_{22}^0, \boldsymbol{\theta}_{22}^0)} \\ &= \frac{1}{|\mathcal{B}_{k_2}|} \sum_{i \in \mathcal{B}_{k_2}} \nabla_{\mathbf{M}_2, \boldsymbol{\theta}_2} (\mathcal{L}_{\mathbf{M}_1^0, \boldsymbol{\theta}_1^0}[\mathbf{y}_i, \mathbf{x}_i] - \mathcal{L}_{\mathbf{M}_2, \boldsymbol{\theta}_2}[\mathbf{y}_i, \mathbf{x}_i])|_{(\mathbf{M}_2, \boldsymbol{\theta}_2) = (\mathbf{M}_{22}^0, \boldsymbol{\theta}_{22}^0)} \\ &= -\frac{1}{|\mathcal{B}_{k_2}|} \sum_{i \in \mathcal{B}_{k_2}} \nabla_{\mathbf{M}_2, \boldsymbol{\theta}_2} \mathcal{L}_{\mathbf{M}_2, \boldsymbol{\theta}_2}[\mathbf{y}_i, \mathbf{x}_i]|_{(\mathbf{M}_2, \boldsymbol{\theta}_2) = (\mathbf{M}_{22}^0, \boldsymbol{\theta}_{22}^0)}. \end{aligned}$$

The individual gradients $\nabla_{\mathbf{M}, \boldsymbol{\theta}} \mathcal{L}_{\mathbf{M}, \boldsymbol{\theta}}[\mathbf{y}_i, \mathbf{x}_i]|_{(\mathbf{M}, \boldsymbol{\theta}) = (\mathbf{M}^0, \boldsymbol{\theta}^0)}$ can then be computed by back propagation [40].

B Convergence

Proposition 1 (Convergence). *If there exist parameters $(\mathbf{M}, \boldsymbol{\theta}) \in (\mathcal{M}, \Theta)$ that make the objective function given in (6) equal to zero, Algorithm 1 is guaranteed to converge.*

Proof. The proof follows readily from [31, 44]. \square

The assumption of parameters for a perfect fit can be relaxed, but in this paper, we are interested less in the mathematical details of our specific algorithm but rather in showing that the MoM approach works in the first place. Our numerical studies in the main part of the paper serve this purpose.

C The case $b = 1$

In the case $b = 1$, by definition, we have

$$\widehat{\mathbf{W}}_{\text{MoM}}^{\mathcal{B}_1} \in \arg \min_{(\mathbf{M}_1, \boldsymbol{\theta}_1) \in (\mathcal{M}, \Theta)} \left\{ \frac{1}{n} \left(\sum_{i=1}^n \mathcal{L}_{\mathbf{M}_1, \boldsymbol{\theta}_1}[\mathbf{y}_i, \mathbf{x}_i] - \sup_{(\mathbf{M}_2, \boldsymbol{\theta}_2) \in (\mathcal{M}, \Theta)} \mathcal{L}_{\mathbf{M}_2, \boldsymbol{\theta}_2}[\mathbf{y}_i, \mathbf{x}_i] \right) \right\},$$

which implies that $\widehat{\mathbf{W}}_{\text{MoM}}^{\mathcal{B}_1}$ is equivalent to the minimizer of $\sum_{i=1}^n \mathcal{L}_{\mathbf{M}_1, \boldsymbol{\theta}_1}^{\text{SE}}[\mathbf{y}_i, \mathbf{x}_i]/n$ or $\sum_{i=1}^n \mathcal{L}_{\mathbf{M}_1, \boldsymbol{\theta}_1}^{\text{SCE}}[\mathbf{y}_i, \mathbf{x}_i]/n$.

D Details on the computations

The computations in this paper were performed using R programming language [38] with Nvidia K80s GPUs; Table 6 shows the calculation time for one set of simulations in Table 1, which was described in Section 4.2 on a single GPU; Table 7 shows the error bar in terms of standard deviation over 20 runs.

Table 6: computation time (hour) for one set of simulation.

Corrupted outputs: uniform distribution				
Computation time				
$ \mathcal{I} /n$	MoM _{min}	AD	Huber _{min}	SE
100%	2.14	0.24	0.60	1.38
95%	1.25	0.23	0.37	0.63
85%	1.66	0.24	0.57	0.19
75%	0.74	0.24	0.93	0.66

Corrupted outputs: t-distribution				
Computation time				
df	MoM _{min}	AD	Huber _{min}	SE
10	1.78	0.23	0.46	1.17
1	2.23	0.23	0.55	1.51

Corrupted inputs				
Computation time				
$ \mathcal{I} /n$	MoM _{min}	AD	Huber _{min}	SE
95%	2.14	0.25	0.58	1.35
85%	2.78	0.23	0.48	1.29
75%	2.17	0.24	0.84	1.07

Table 7: standard deviation for one set of simulation over 20 runs.

Corrupted outputs: uniform distribution				
Standard deviation				
$ \mathcal{I} /n$	MoM _{min}	AD	Huber _{min}	SE
100%	2	2	2	1
95%	2	2	3	3
85%	2	2	5	5
75%	3	3	6	6

Corrupted outputs: t-distribution				
Standard deviation				
df	MoM _{min}	AD	Huber _{min}	SE
10	2	1	2	1
1	2	5	2	1

Corrupted inputs				
Standard deviation				
$ \mathcal{I} /n$	MoM _{min}	AD	Huber _{min}	SE
95%	2	2	2	1
85%	2	2	2	1
75%	2	1	2	1